Surfaces and Interfaces in Nanostructured Materials II
Edited by S.M. Mukhopadhyay, N.B. Dahotre, S. Seal, and A.Agarwal
TMS (The Minerals, Metals & Materials Society), 2006

Synthesis of nanocrystalline intermetallic layer by mechanical attrition

X. Wu[1,2,3], Y. Hong[1], N. Tao[2], X. K. Meng[4], J. Lu[3] and K. Lu[2]

[1] State Key Laboratory of Nonlinear Mechanics, Institute of Mechanics, Chinese Academy of Sciences, Beijing 100080, China
[2] Shenyang National Laboratory for Materials Sciences, Institute of Metal Research, Chinese Academy of Sciences, Shenyang 110016, China
[3] Department of Mechanical Engineering The Hong Kong Polytechnic University Hung Hom, Kowloon, Hong Kong, China
[4] Department of Materials Science, Nanjing University, Nanjing 210093, China

Keywords: nanocrystalline, diffusion, intermetallics, surface mechanical attrition treatment.

Abstract

By means of the technique of surface mechanical attrition treatment, the nanocrystalline (nc) intermetallic compound Co3Fe7 was synthesized in the surface layer of bulk cobalt. It was found that deformation-induced diffusion occurred, leading to the extension of solid solution. A series of phase transformation proceeded with increasing Fe content (atom %) and followed the route from hcp (< 4% Fe) to fcc (4~11% Fe) and finally to bcc (> 11% Fe). Nanoscale composition analyses by EDX showed that Fe contents are significantly higher in grain boundaries and triple junctions than in grain interiors. It was turned out to be the conclusion that fast diffusion along grain boundaries dominate in larger grains whereas diffusion along triple junctions in nc intermetallic grains. The alloying on the atomic level was ascribed to deformation-induced intermixing during deformation at high strain rates. The mechanism of intermetallic formation was a result of numerous nucleation events followed by limited growth.

Introduction

The nanocrystalline (nc) metallic materials produced by severe plastic deformation (SPD) exhibit the superior diffusional property due to the effect of both grain boundaries (GBs) and triple junctions (TJs) of high volume fraction [1-6]. These GBs are in a high-energy non-equilibrium state [1,4], with GB diffusion coefficients being several orders of magnitude larger than those in nc materials fabricated by non-mechanical (more equilibrium than mechanical) methods and in conventional polycrystallites [1,2,5,6]. The TJs have weaker bonding structures compared with GBs and consequently higher diffusivity [7]. Diffusion along TJs will dominate in nc grains with grain sizes less than ~10 nm where the TJ density is enhanced significantly [7,8]. On the other hand, the high-density defects, such as dislocations dramatically created during SPD also contribute significantly fast diffusion. The dislocations provide pipe diffusion via the core of dislocations due to the decrease of the vacancy formation energy in dislocation cores [9]. Meanwhile, SPD may induce vacancies and increase the mobile vacancy concentration [10-12]. The high level of vacancies may induce pronounced enhancement of diffusivity during SPD and their concentration will be proportional to both strain rate and dislocation density [13].

SPD-induced diffusion may promote the formation of a wide spectrum of highly non-equilibrium states in nc materials. The formation of supersaturated solid solutions in immiscible Al-Fe alloys and pearlitic steel [14,15], disordering or even amorphization of

intermetallics [16], and alloying in Cu-Fe composite [11] have been reported during high-pressure torsion. In the present study, an nc intermetallic layer was synthesized via in situ alloying during surface mechanical attrition treatment (SMAT). The strategy was to generate the nc surface layer with novel phase structures, e.g. intermetallic compound, different from the metallic matrix via deformation-induced atom diffusion that occur in situ during the plastic deformation process. This nc layer is free of contamination and porosity because of the self-nanocrystallization induced by severe surface plastic deformation. The microstructural responses with strain were investigated in detail, including solid solution extension, phase transformation, and nc intermetallic formation. The Fe-Co system was selected due to their unlimited solubility range, which is convenient for correlating the formation of various non-equilibrium states with relative composition change during plastic deformation.

Experimental

The material used in this study was an electrodeposited cobalt plate (purity: 99.98 wt%). The average grain size was ~30 μm. The shape of specimen was 100×100×5 mm.The SMAT technique was used to realize the SPD-induced diffusion process. The SMAT technique has been described in our previous papers [17]. In brief, the specimen was placed in a cylinder-shaped stainless steel chamber with a large number of hardened steel balls inside. The chamber was attached to a vibration generator and during SMAT the balls were resonated because of the high vibration frequency of the system. Flying balls peened the specimen surface repetitively and imposed severe strains into the surface layer, leading to progressive refinement of grains to the nanoscale regime. Diffusion is anticipated to occur simultaneously during deformation from balls into the specimen surface as the same as in conventional mechanical alloying process [18]. Moreover, both strain and strain rate had a gradient variation from the treated surface (both are extremely large) towards the deep matrix (essentially zero), and as a result, the grain sizes with gradient distribution were developed in the treated sample [19,20]. In the present work, the SMAT process was performed at room temperature with a vibrating frequency of 50 Hz in a vacuum for 50 minutes. The hardened steel ball had a diameter of 8 mm and a composition (wt%) of 1.35 Cr, 0.98 C, base Fe.

Following SMAT, the microstructural characterization was performed in a scanning electron microscope (SEM) and a field emission gun transmission electron microscope (TEM). Both planar-view and cross-sectional thin foils for TEM observations were prepared by means of cutting, grinding, dimpling and a final ion thinning or twin-jet polishing at low temperatures. A beam size of about 2 nm and a typical spectrum of collecting time of 100 s were used to the nanoscale energy dispersive X-ray (EDX) spectroscopy analysis. X-ray diffraction (XRD) analyses were conducted to determine the phase constitution within the treated layer.

Experimental results

Figure 1 shows XRD patterns prior to and after SMAT. The matrix cobalt has a hexagonal close packed (hcp) structure. In contrast, a single body center cubic (bcc) phase is present in the treated layer of ~20 μm thick. This bcc phase is determined to be intermetallic compound Co3Fe7. The SEM cross-section of the treated layer is shown in Figure 2. The layer of ~20 μm thick exhibits a typical interlayer structure, much similar to that in MA [18]. The composition measurement indicates introduction of both Fe and Cr in the treated layer. Hence, the alloying process occurs during deformation.

The microstructure in the treated layer was investigated by cross-sectional TEM observations. Figure 3(a) is a bright-field image (~5 μm deep from the treated surface), showing the presence of nc grains. Figs. 3(b) and (c) are the electron diffraction pattern (EDP) and EDX

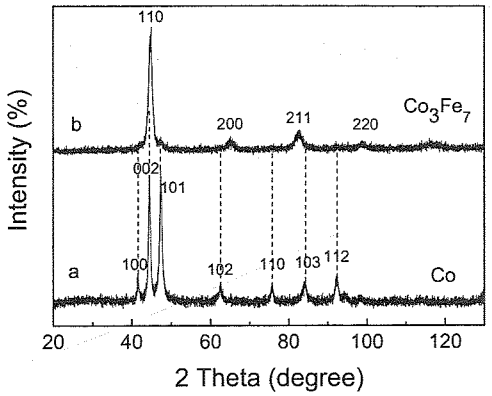

Fig. 1 X-ray diffraction patterns.

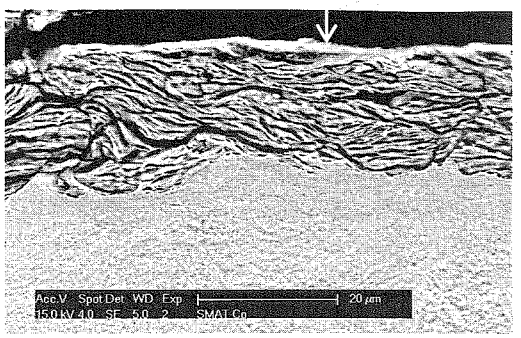

Fig. 2 SEM image of the treated layer

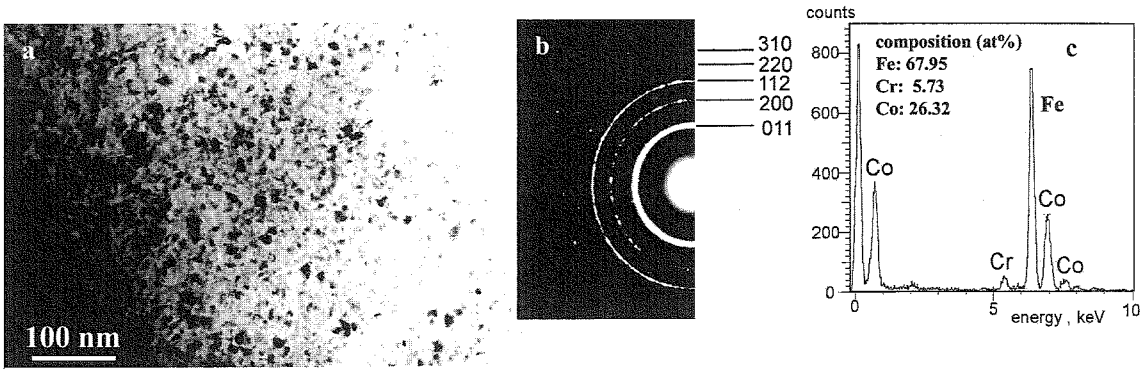

Fig. 3 (a) TEM micrograph of nc Co3Fe7 (~5 μm deep). (b) EDP. (c) EDX spectrum

spectrum of Co3Fe7 respectively. Note the presence of a few amount of Cr. TEM observations at various depths confirm the formation of intermetallic Co3Fe7 within the treated layer, consistent with XRD result.

In order to clarify the microstructural evolution relative to intermetallic formation, the interface between the intermetallic layer and cobalt is investigated in detail via cross-sectional TEM observations. Figure 4(a) is the microstructure located exactly at interface (~20 μm deep). A clear change in grain sizes is visible at the interface. The submicron-sized grains at the right side are determined to be hcp cobalt, with stacking faults in their interiors. The nc grains at left side are Co3Fe7. Figs. 4 (b) and (c) are EDPs of Co3Fe7 and cobalt respectively, both revealing a ring-like feature of random orientations among grains.

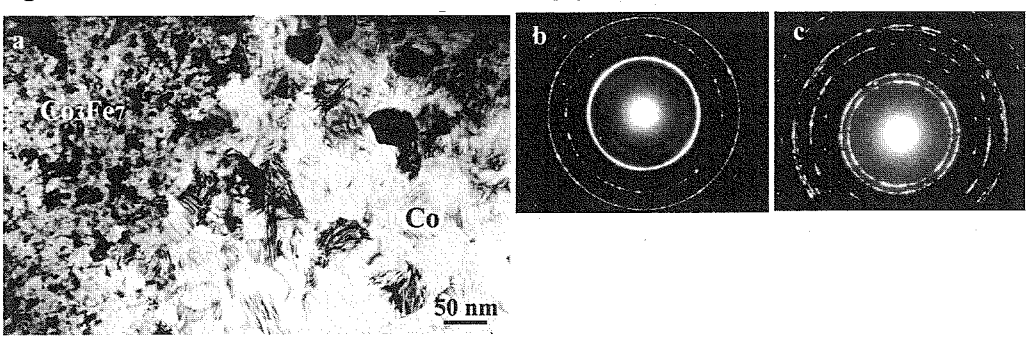

Fig. 4 (a) Cross-sectional TEM micrograph at interface between intermetallic layer and cobalt (~20 μm deep). (b) and (c) EDPs of Co3Fe7 and cobalt.

Of particular interest is the finding that a transition zone exists between intermetallic layer and cobalt. Fig. 5 shows EDX spectra and corresponding EDPs obtained in three grains located

in sequence from cobalt to intermetallic. Three kinds of crystal structures are visible, i.e. hcp (a), fcc (b) and bcc (c), respectively, with Fe (Cr) contents (atom %) of 1.67 (0.23), 9.40 (1.42) and 23.09 (1.37) %. This indicates the extension of solid solution and a series of phase transformations occurring due to diffusion of Fe (Cr) into cobalt in the transition zone. Extensive EDX measurements show that cobalt will keep hcp structure with increasing Fe content (atom %) to ~ 3.9% Fe, then change to fcc with 4 ~ 11% Fe, and finally to bcc with further increased Fe content. Hence, the sequence of phase transformations can be represented relevant to Fe contents (atom %) as: hcp (< 4 Fe) → fcc (4~11 Fe) → bcc (> 11 Fe). This result has relative small deviations compared with the Co-Fe equilibrium phase diagram extrapolating to room temperature [21].

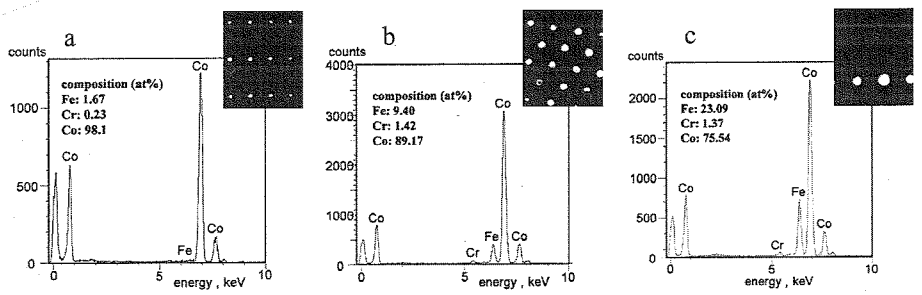

Fig. 5 EDX spectra and corresponding micro-diffractions showing the change of the crystal structure from hcp (a) to fcc (b) and to bcc (c) due to an increase in Fe(Cr) contents within the transition layer.

The initial formation of intermetallic Co3Fe7 was further investigated. Figure 6(a) shows a number of nc Co3Fe7 grains together with several larger grains. Inset in Figure 6(b) is the microdiffraction pattern of the grain labeled A. A set of well-defined bcc diffraction spots together with a ring of bcc Co3Fe7 is visible. The dark-field image of grain A in Figure 6(b) shows numerous extremely small nc Co3Fe7 grains. The microscopic analyses by EDX show inhomogeneous Fe compositions at the atomic level in grain A, ranging from 16.27 to 57.36 atom %. This gives clear evidence that the intermetallic Co3Fe7 nucleate directly in a bcc solid solution. Both solid solution extension and phase transformation occur prior to intermetallic formation.

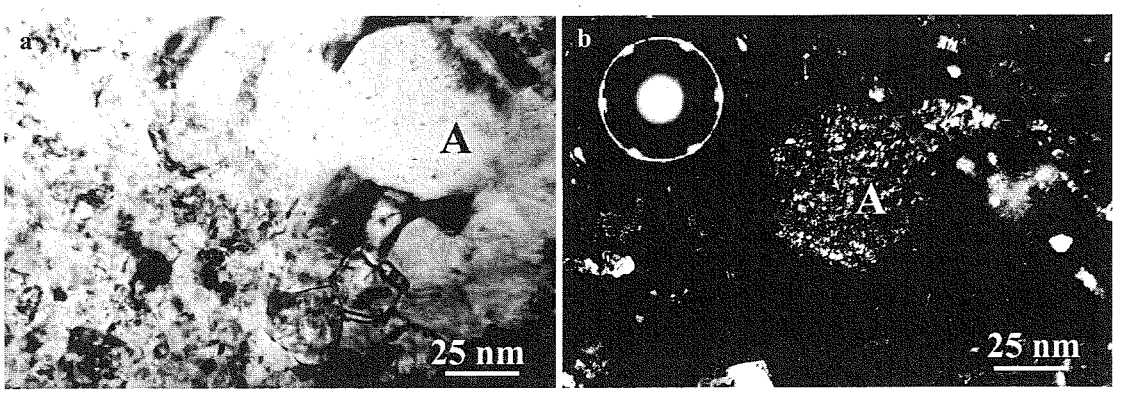

Fig. 6 Cross-sectional TEM observation at the interface (~20 μm deep). (a) Bright-field image. (b) Dark-field image showing the existence of nc grains inside grain A. Inset is the micro-diffraction from grain A.

The composition analyses by EDX were made in both transition zone and intermetallic layer in order to shed light on the nature of diffusion related to grain sizes. Figure 7 summarizes composition data in TJs, SFs, GBs, and grain interiors (GIs) in FCC and BCC structures. Clearly,

Fe (Cr) contents increase in sequence at GIs, GBs and TJs.

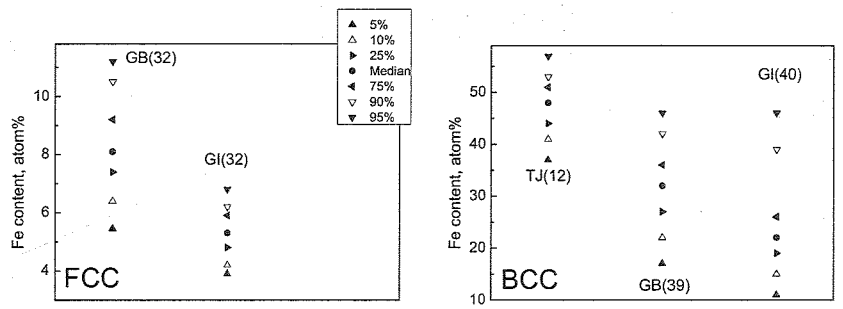

Fig. 7 EDX composition data of Fe contents in SFs, GBs, GIs, and TJs in FCC and BCC phases. The number in bracket indicates the whole measured values.

The hardness by the nanoindentation test is plotted in Figure 8 as a function of the depth of the treated layer. The values of hardness in intermetallic layer ranges from 14 to 12 GPa, much higher than 6.2 GPa of cobalt.]

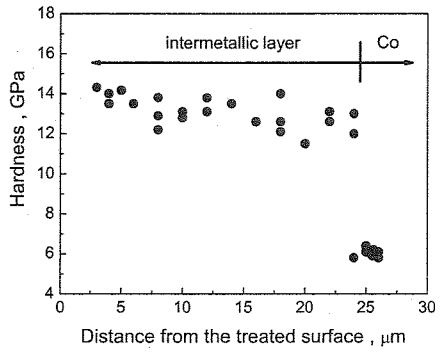

Fig. 8 Hardness along the layer depth.

Discussion

The repetitive peening of shots refines grains and produces fresh ball/specimen surfaces during the SMAT process. Taking into consideration of rapid impact velocity and high impact frequency of shots, diffusion of Fe (Cr) may occur from balls and the steel container walls into the treated surface of specimen, as in the case of MA [18].

Diffusion occurs first in hcp grains of cobalt and then in hcp, fcc, and bcc solid solution in the transition zone, as shown in Fig. 9. The hcp grains are submicro-sized whereas fcc and bcc grains range at large end of nanoscale regime (50-100 nm). From composition data in Fig. 7, Fe contents in GBs are much higher than in grain interiors. The GBs of severely deformed grains are characterized by a highly nonequilibrium high-energy state. The energy stored in GBs may facilitate diffusion along GBs for decreasing the defect formation energy [2-4]. Furthermore, GB diffusion in nc materials produced by SPD is determined mainly by GB state rather than by the mean grain size and therefore, fast GB diffusion may occur even in grains beyond the nanoscale [2,3]. Meanwhile, due to the much high volume fraction of GBs compared with that of TJs for larger grains, it is reasonable that GB diffusion dominates in the transition zone.

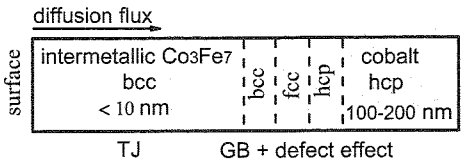

Fig. 9 Schematic illustration of the microstructural evolution during the SMAT process. Note the presence of a transition zone containing hcp, fcc, and bcc solid solution due to diffusion and phase transformation.

With the advent of nc Co3Fe7, the volume fraction of TJs will increase drastically due to grain sizes of less than 10 nm [6,7]. Because TJs structurally have a loosely bonded nature and a large excess volume compared to GBs, diffusion along TJs will be much facilitated in the intermetallic layer. The occurrence in the bulk of a continuous network of TJs assists a creation of short diffusion paths.

The plastic deformation may increase mobile vacancy concentration [11,12]. The vacancy formation energy and internal stress as well are two parameters controlling the vacancy formation. The vacancy formation energy is significantly lowered in nc grains [22]. The internal stress due to the compressive strain during the SMAT process may promote the formation of excess vacancies by reducing the vacancy formation energy [11]. The rate of production of vacancies will be proportional to strain rate. The experimental data of Kiritani et al [23] showed that at a strain rate of ~1 s^{-1} during ~1 s, the vacancy concentration in copper at room temperature rises up to 10^{-5} leading to vacancy cluster formation. During the HPT process of a Cu-Fe filamentary composite, the mobile vacancy concentration and vacancy diffusion coefficient are estimated to increase by 15 and 4 orders of magnitude, respectively, providing an additional mobile vacancy production rate of 10^{-5} s^{-1} [11]. This high level of vacancies increases the diffusion coefficient, leading to true alloying to occur at the atomic level during the HPT process. The SMAT process provides a higher strain rate (10^{3-4} s^{-1} [17]) than HPT. It is, therefore, reasonable that the mobile vacancy concentration may be greatly enhanced.

The specimen will experience temperature rise due to large strains and high strain rates during the SMAT process similar to the case in MA [18]. The exact temperature on the top treated surface is difficult to evaluate, however, due to the dynamic nature of the SMAT process. In spite of differences between SMAT and MA, one may find clues on temperature rise in the case of MA. From data available on the measured temperatures during MA, the macroscopic maximum temperature is ~ 215°C, and more commonly it is ~100-120°C, even though local temperature (microscopic) can be higher. This suggests that there is only a moderate temperature rise during SMAT and that microscopic temperatures are probably much below the recrystallization temperature. Hence, the process of diffusion during SMAT is mechanically-controlled.

The CoFe system has very small negative heat of mixing of about –1 kJ/mol [24]. Previous MA of elemental Fe and Co powders produced the intermetallic Co50Fe50 [25]. The nature of MA of Co and Fe powders is the mixing of the elements by interdiffusion [26]. In the present study, true alloying on the atomic level can be achieved through gradual diffusive intermixing. The deformation-assisted diffusion plays a significant role in controlling the alloying process. The formation of nc intermetallic Co3Fe7 is a direct result of numerous nucleation events with limited growth of grains, as shown in Fig. 6.

This work has shown a new route concerning an alloying process on the surface of metallic materials that eliminate different phases of preparation of intermetallic materials. By this

approach new nc materials are able to be prepared directly with a judicious selection of the composition of the target materials, e.g. the shot, atmosphere, and medium of the working chamber. The development of new structures and functional materials is, thus, anticipated.

Conclusions

(1) The nanocrystalline intermetallic compound Co3Fe7 was generated in the treated layer during surface mechanical attrition treatment of bulk cobalt. A transition zone existed between the intermetallic layer and cobalt where the extension of solid solution and a series of phase transformation occur.
(2) Diffusion happened in various solid solutions. Nanoscale composition analyses by EDX showed that Fe contents are significantly higher in GBs and TJs than in grain interiors. Diffusion along GBs dominate in larger grains whereas diffusion along TJs in nc intermetallic grains.
(3) The alloying process was ascribed to intermixing at the atomic scale during severe deformation. The mechanism of intermetallic formation was a result of numerous nucleation events.

Acknowledgements

This research received backing from Natural Science Foundation of China Grant No. 50471086, 10472117 and 50021101, National Basic Research Program of China Grant No. 2004CB619305, the Chinese Academy of Sciences Grant No. KJCX2-SW-L2, and National Center for Nanoscience and Technology, China.

References

1. R. Wurschum, U. Brossmann, H.E. Schaefer. in Nanostruct Mater, ed. C.C. Koch, Noyes Pubs, Norwich, New York, USA, (2001), p.267.
2. M.D. Baro, YU.R. Kolobov, I.A. Ovid'ko, H.E. Schaefer, B.B. Straumal, R.Z. Valiev, H.R. Alexandrov, M. Ivanov, K. Reimann, A,B.Reizis, S. Surinach, A.P. Zhilyaev, *Rev Adv Mater Sci*, 2 (2001), 1.
3. R. Wurschum, S. Herth, U. Brossmann, *Adv Eng Mater*, 5 (2003), 365.
4. Y.R. Kolobov, G..P. Grabovetskaya, M.B. Ivanov, A.P. Zhilyaev, R.Z. Valiev, *Scr Mater* ,44 (2001), 873.
5. Z.B. Wang, N.R. Tao, W.P. Tang, J. Lu, K. Lu, *Acta Mater*, 51 (2003), 4319.
6. Z.B. Wang, J. Lu, K. Lu, *Acta Mater*, 53 (2005), 2081.
7. H.T. Wang, W. Yang, A.H.W. Ngan, *Scripta Mater*, 52 (2005), 69.
8. G. Palumbo, S.J. Thorpe, K.T. Aust. *Scr Metall Mater*, 24 (1990), 1347.
9. D. Turnbull, R.E. Hoffman, *Acta Mater*, 2 (1954), 419.
10. Van Petergem S, Dalla Torre F, D. Segers, Van Swygenhoven H,. *Scr Mater*, 48 (2003), 17.
11. X. Sauvage, F. Wetscher, P. Pareige, *Acta Mater*, 53 (2005), 2127.
12. B.B. Straumal, B. Baretzky, A.A. Mazilkin, F. Phillipp, O.A. Kogtenkova, M.V. Volkov, R.Z. Valiev, *Acta Mater*, 52 (2004), 4469.
13. K.L. Murty, K. Detemple, O. Kanert, J.T.M. Dehosson, *Metal Mater Trans A*, 29 (1998), 153.
14. A.A. Nazarov, A.E. Romanov, R.Z. Valiev, *Acta Metall Mater*, 41 (1993), 1033.
15 Ivanisenko Yu, W. Lojkowski, R.Z. Valiev, H.J. Fecht, *Acta Mater*, 51 (2003), 5555.
16. A.V. Korznikov, O. Dimitrov, G.F. Korznikova, J.P. Dallas, A. Quivy, R.Z. Valiev, *NanoStruct Mater*, 11 (1999), 17.
17. K. Lu and J. Lu, *J Mater Sci Technol* 15 (1999), 193. *Mater Sci Eng A*, 375-77 (2004), 38.
18. C. Suryanarayana, *Int Mater Rev*, 40 (1995), 41; *Prog Mater Sci*, 46 (2001), 1.
19. X. Wu, N. Tao, Y. Hong, G. Liu, B. Xu, J. Lu, K. Lu, *Acta Mater*, 53 (2005), 681.
20. Wu X, Tao N, Hong Y, Lu J, Lu K.Scripta Mater 2005;52:547.

21. N. Mattoso, N. Fernandes, M. Abbate, W.H. Schreiner, D.H. Mosca, *Electrochemical and Solid-State Lett*, 4 (2001), C20.
22. W.H. Qi, M.P. Wang, *J Mater Sci*, 39 (2004), 2529.
23. M. Kiritani, K. Yasunaga, Y. Matsukawa, M. Komatsu, *Radiat Effects Defects Solids*, 157 (2002), 3.
24. A.K. Niessen, de Boer FR, R. Boom, de Chatel PF, W.C.M. Mattern, A.M. *Miedema. CALPHAD,* 7 (1983), 51.
25. R. Elkalkouli, M. Grosbras, J.F. Dinhut, *NanoStruct Mater*, 5 (1995), 733.
26. R. Bruning, K. Samwer, C. Kuhrt, L. Schultz, *J Appl Phys*, 72 (1992), 2978.